Journal of Medicinal Chemistry

Article

A Lipophilic Pt(IV) Oxaliplatin Derivative Enhances Antitumor Activity

Aiman Abu Ammar, Raji Raveendran, Dan Gibson, Taher Nassar, and Simon Benita

J. Med. Chem., **Just Accepted Manuscript** • DOI: 10.1021/acs.jmedchem.6b00955 • Publication Date (Web): 07 Sep 2016

Just Accepted

ACS Publications

Journal of Medicinal Chemistry is published by the American Chemical Society. 1155 Sixteenth Street N.W., Washington, DC 20036

A Lipophilic Pt(IV) Oxaliplatin Derivative Enhances Antitumor activity

*Aiman Abu Ammar, Raji Raveendran, Dan Gibson, Taher Nassar[†] and Simon Benita[†]**

The Hebrew University of Jerusalem, Institute for Drug Research of the School of Pharmacy, Faculty of Medicine, POB 12065, Jerusalem, 9112100, Israel

ABSTRACT

Side effects and acquired resistance by cancer cells limit the use of Platinum (Pt) anticancer drugs. Modification of oxaliplatin (OXA) into a lipophilic Pt(IV) complex [Pt(DACH)(OAc)(OPal)(ox)] (**1**), containing both lipophilic and hydrophilic axial ligands, was applied to improve performance and facilitate incorporation into polymeric nanoparticles. Complex **1** exhibited unique potency against a panel of cancer cells, including cisplatin-resistant tumor cells. [Pt(DACH)(OAc)(OPal)(ox)] incorporated nanoparticles (**2**) presented a mean diameter of 146 nm with encapsulation yields above 95% as determined by HPLC. **1** and **2** showed enhanced *in vitro* cellular Pt accumulation, DNA platination and anti-proliferative effect compared to OXA. Results of an orthotopic intraperitoneal model of metastatic ovarian cancer (SKOV-3) and a xenograft subcutaneous model of colon (HCT-116) tumor in SCID-bg mice showed that the activity of **1** and **2** significantly decreased tumor growth rates compared to control and OXA treatment groups. Consequently, these findings warrant further development towards clinical translation.

Keywords: Nanoparticles; Oxaliplatin; Lipophilicity; Prodrug; Pt(IV) derivative

1. INTRODUCTION

Cancer is considered to be one of the main causes of death in the world. While chemotherapy continues to be the mainstay treatment for cancer, it is closely linked with considerable mortality and morbidity rates especially due to non-specific damage to normal cells[1]. The clinical success of cisplatin has played an instrumental role in the development of Pt anticancer compounds. With the purpose of searching for safer and more effective Pt-based compounds, numerous efforts have been made in the past decades. However, only a few of these complexes have entered clinical trials. Two of these, carboplatin and oxaliplatin (OXA) have been approved by the FDA and are currently being used worldwide for malignant tumor chemotherapy[2].

OXA is a diaminocyclohexane (DACH) derivative of cisplatin however, the spectrum of activity of OXA differs from cisplatin and includes several lines of colon, ovarian, and lung cancer, as well as cell lines that are resistant to Pt therapy. OXA was the first Pt-based drug approved for use against metastatic colorectal cancer in combination with fluorouracil and leucovorin. OXA interferes with DNA replication and transcription systems through nuclear DNA adduct formation. Despite its better tolerability compared to other Pt compounds, OXA is also associated with side effects such as neurotoxicity, hematologic and gastrointestinal tract toxicities, neutropenia, nausea, and vomiting that limit the range of usable doses [3]. Hence, novel Pt complexes displaying increased anti-tumor activity and reduced cross-resistance are still being sought.

Pt(IV) complexes are a new generation of Pt-based drugs, possessing markedly different properties from those of Pt(II) compounds. The kinetic inertness prevents the conversion to off-target biological substances before the Pt complex can reach the

nuclear DNA. Furthermore, the two additional ligands can be utilized and tuned to adjust the chemical properties and facilitate the incorporation of Pt compounds into nanoparticles. These features can potentially improve both the efficacy and tolerability profile of Pt complexes [4]. The strategy for the preparation of Pt(IV) complexes involves oxidative addition of the square planar Pt(II) complexes, usually with hydrogen peroxide, to yield axial hydroxide ligands which can be carboxylated or carbamated with the aim of introducing a versatile axial ligands [5-7]. The reduction to Pt(II) is a paramount demand for binding to the targeted biological sites. Thus, the reduction potential of the Pt(IV) complexes as well as the redox status of the tumor environment have a strong impact on the activity of Pt(IV) anticancer drugs [8]. Pt(IV) drugs are generally regarded as prodrugs due to the disparity in reactivity prior to and following reduction[4]. Solubility and lipophilicity have a crucial role in designing new Pt(IV) compounds. Numerous studies have shown a good correlation between lipophilicity and cytotoxicity [9-11]. Even though it has a critical role in enhancing the cytotoxic activity of the prodrug, lipophilicity is not the main factor, which determines the overall activity. Moreover, high lipophilicity usually leads to low water solubility, making the drug formulation in an aqueous solution difficult. The low aqueous solubility has been always considered a stumbling block to the development and clinical use of anticancer compounds, due to the intravenous (i.v.) infusion route of their administration. Poorly water-soluble anticancer drugs need to be formulated in co-solvents and/or surfactant solutions to enhance their solubility, but many of these solutiuons, which have been used for solubilization such drugs, are responsible for the severe side effects. The classic examples for these formulations are the marketed taxane products, paclitaxel and docetaxel which have had a profound effect in a wide variety of malignancies. In the case of paclitaxel, a polyoxyl-35 castor

oil surfactant vehicle is used in the commercial formulation. Its presence triggers severe hypersensitive reactions in patients and it has been reported that 30–40% of the patients receiving paclitaxel suffer from abnormal lipoprotein patterns, aggregation of erythrocytes, severe hypersensitive reactions and peripheral neuropathy [12-14]. Similarly, ethanol and polysorbate 80, used for docetaxel solubilization also lead to adverse effects [15-17]. Thus, there is a clear need to compromise between lipophilicity and solubility. Well-designed drug delivery systems are essential if we wish to continue to clinical practice[18].

Nanoparticles (NPs) are particulate dispersions or solid particles possessing dimensions of 1-1000 nm, with the capability to transport and deliver medicinal substances to selected targets within biological systems[19]. A large number of nanotherapeutics have been designed and evaluated over the years, relying on liposomes, polymers, micelles, NPs and antibodies as carrier materials [20]. Due to their miniscule and colloidal nature, polymer-based NPs are considered an ideal transport vehicle for drugs and other therapeutic agents as the agent can be encapsulated within or conjugated onto the NP's surface[21]. Several methods for polymeric NP preparation have been developed. Amongst them, the nanoprecipitation technique, also known as the solvent displacement method, exhibits manifest advantages, essentially because it is a one-step process and easy to perform at room temperature [22]. Owing to their size, NPs preferentially target solid tumors rather than healthy tissues by exploiting vasculature inadequacy [23]. One of the clinically successful candidates was the albumin-based formulation of paclitaxel NPs. It was developed with the aim of overcoming the very low solubility of paclitaxel, to form nab-paclitaxel NPs with a mean particle size of 130 nm. The resulting marketed paclitaxel nanoparticulate

formulation is water-dispersible and was first approved by the FDA in 2005 for the treatment of metastatic breast cancer.

This study presents the development and characterization of a drug delivery system loaded with a potent Pt(IV) prodrug of OXA, [Pt(DACH)(OAc)(OPal)(ox)] (**1**) (Scheme 1), as well as handling properties of NPs before and after freeze drying and storage. The cytotoxicity, Pt accumulation, and DNA platination of **2** was evaluated *in vitro* in comparison to **1** and OXA. Furthermore, two *in vivo* studies were conducted in SCID-bg mice including: an orthotopic intraperitoneal (i.p.) model of metastatic ovarian cancer, and a subcutaneous xenograft model of colon cancer.

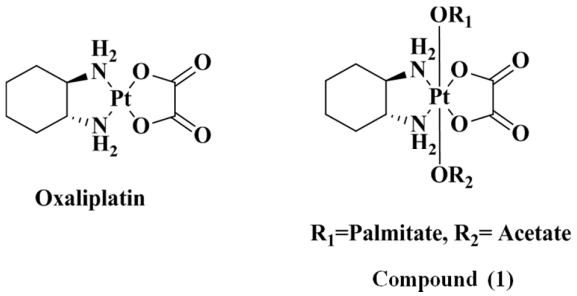

Scheme 1. Structure of OXA and lipophilic Pt(IV) compound **1**.

2. RESULTS

2.1. In vitro cytotoxic activity

The anti-proliferative activities of **1** and OXA were tested in PC-3, PC-3-luc (human prostate cancer), BxPC-3 (human pancreatic cancer), OVCAR-8, SKOV-3 (human ovarian cancer), CT-26-luc (murine colorectal cancer) cell lines by the MTT assay. The cells were treated continuously over 120h. The 50% growth inhibitory concentration (IC_{50}) values were calculated and summarized in Table 1. Complex **1** showed a unique potency against different cancer cell lines, with higher cytotoxicity than OXA.

The activity of OXA and **1** against a pair of cisplatin-sensitive and resistant ovarian cancer cell lines, A2780 and A2780-cisR, was determined as a function of the concentration. The resistance of A2780cisR to cisplatin is achieved by reducing the uptake, improving DNA repair and increasing glutathione levels.

Table 1. IC_{50} values of OXA and **1** in various cancer cell lines.

Cell line	IC_{50} (μM)[a]	
	OXA	**1**
PC-3	9.2±0.4	0.35±0.01
PC-3-luc	27.7±9.1	0.46±0.11
BxPC-3	3.4±0.9	0.35±0.01
OVCAR-8	9.4±4.4	0.46±0.03
SKOV-3	58.3±6.3	0.54±0.03
CT-26-luc	5.6±0.6	0.62±0.24

[a] Values are means ± SD obtained from three independent experiments.

The resistance factor (RF) is defined as the ratio of IC_{50} value in the resistant cell line to that in the parent cell line. The RF values of cisplatin, OXA, and **1** were 15.53, 5.21, and 0.93, respectively (Table S1). The results show that **1** has the lowest RF values, which indicates that **1** can overcome acquired resistance to cisplatin and exhibit efficient activity against the A2780-cisR line and probably against other cancer cell lines that are typically resistant to Pt therapy.

2.2. Preparation and characterization of 2

The preparation of **2** was carried out using the well-established solvent interfacial deposition method resulting in the formation of spherical NPs (Figure 1). The mean

diameter of **2** was about 146nm with polydispersity index (PDI) of 0.1, and the zeta potential value of **2** was approximately -49mV. Furthermore, optimal encapsulation yields were achieved (>95% as determined by HPLC) and incorporation into the NPs ranged from 21.5% to 22.7% w/w. However, because NPs are unstable within aqueous mediums, their clinical use in delivery systems is significantly limited. Freeze-drying is a reliable method to maintain long-term stability for a wide range of biological products such as proteins, peptides or drug-loaded NPs or liposomes [24]. Therefore, after drug encapsulation, formulation **2** was freeze-dried using five cryo- and lyo-protectants; sucrose, (+) trehalose, D (-) mannitol, hydroxypropyl-β-cyclodextrin (HPβCD), and xylitol at different concentrations. Among these, lyophilization of **2** using sucrose (5% w/v) resulted in physically stable NPs. The lyophilized formulation of **2** was stable following incubation at 4°C over a period of 4 weeks, and following incubation at -20°C over a period of 16 weeks (Figure S3). Considering possible clinical issues, the procedures established to freeze-dry **2** appear to be appropriate for the successful development of drug-loaded nanoparticulate formulations intended for parenteral administration. Each batch of **2** was triplicated and the results were similar indicating a good reproducibility of the manufacturing process of the nanoparticles and control of the experimental parameters.

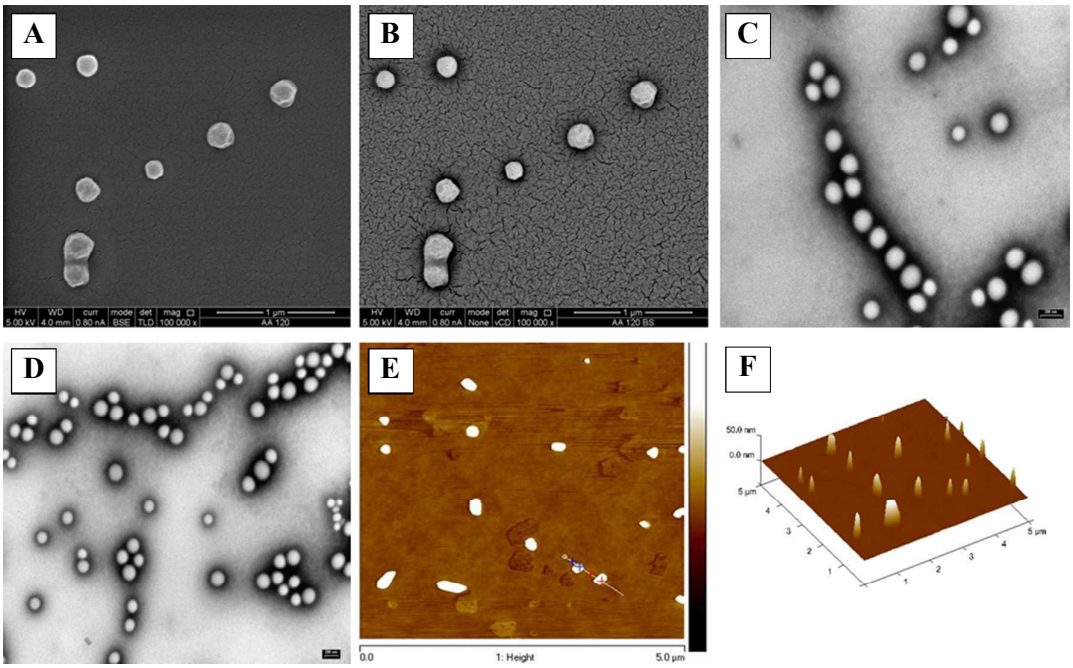

Figure 1. Morphological evaluation of **2**: (A) SEM secondary electron image. (B) SEM backscattered electron image. (C,D) TEM micrographs of uranyl acetate negatively stained NPs at different areas of the grid, scale bar = 200 nm. (E,F) 2D and 3D AFM images of NPs.

Once **1** was successfully encapsulated into NPs, the cytotoxic activity was evaluated in SKOV-3 ovarian cancer cells. The results showed that the cytotoxic activity of **1** and **2** were more pronounced than the toxic activity of OXA, as depicted in Figure S1 and Table S2.

2.3. Cellular uptake, DNA platination and intracellular localization

To examine the cellular accumulation of platinum of OXA, **1** and **2** in cancer cells, the total Pt content was measured by ICP-MS in SKOV-3 cells following their 24h exposure to the compounds at a concentration of 35µM. The data, normalized to the total cellular protein, are presented in Figure 2A. Moreover, the platination of DNA was assessed. Analysis of the extent of DNA platination measured after 24h exposure of SKOV-3 cells to 25µg/mL of OXA (62.5µM), **1** and **2** (35µM), indicated higher

levels of DNA-platination for **1** and **2** in comparison to OXA (Figure 2B). Further cellular uptake studies were carried out to measure the distribution of Pt species in different subcellular fractions. SKOV-3 cells were treated with 35μM of OXA, **1** and **2** for 24h and the cells were fractionated into four compartments: membrane, cytosol, nucleus, and cytoskeleton. The Pt levels in each compartment were measured by ICP-MS. The results are presented in Figure 2C.

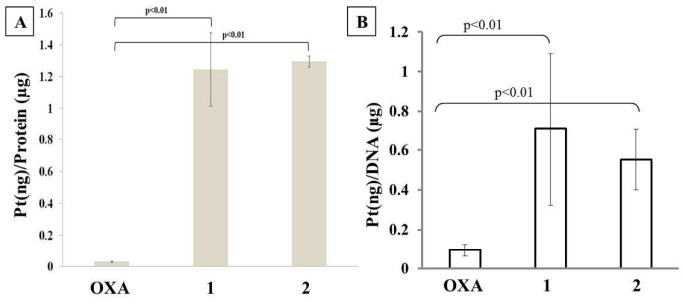

C

Pt (ng)	Membrane	Cytosol	Nucleus	Cytoskeleton
OXA	0.82±0.56	0.11±0.03	0.16±0.21	0
1	68.41±3.53	22.92±0.61	0.73±0.17	0.24±0.06
2	11.74±0.33	5.57±0.25	0.1±0.02	0.26±0.18

Figure 2. (A) Platinum accumulation in whole cells following incubation with 35μM of OXA, **1** and **2** following a 24h exposure to SKOV-3 cells as measured by ICP-MS. Values are the means ± SD obtained from three independent experiments. Statistical analysis revealed that the observed difference in platinum accumulation values was significant (*p<0.01, one-way* ANOVA). (B) The extent of DNA platination following 24h exposure to SKOV-3 cells as measured by ICP-MS. Values are mean ± SD obtained from seven independent experiments. Statistical analysis revealed that the observed difference in DNA platination values was significant (p<*0.01, one-way* ANOVA). (C) Cellular distribution of Pt compounds in different fractions. The amount of Pt per $50x10^3$ cells in cell membrane, cytosol, nucleus and cytoskeleton fractions. Cells were exposed to 35μM of Pt compounds for 24h. Values are means ± SD. Nuclear fraction described by the manufacturer as follows: Total nucleus soluble proteins, including the nuclear membrane proteins. Cytosol Fraction: Total cellular soluble proteins from cytoplasm. Membrane/Particulate: Total cellular membrane proteins including cellular organelles and organelle membrane proteins (excluding the nuclear membrane proteins). Cytoskeletal Fraction: Total cellular insoluble proteins, genomic DNA.

2.4. Cellular uptake of NPs in SKOV-3 cells by CLSM

Localization and cellular uptake of the NPs were evaluated 15 min following incubation (Figure 3A) and was most evident after 6h (Figure 3B). The nucleus was stained by DAPI (blue) whereas the NPs, fluorescently labeled using PE **Lissamine** Rhodamine B (red), were easily visualized within the cytoplasm. Indeed, increased cytoplasmic accumulation of NPs was observed as a function of dilution (1:100 versus 1:200) and time, with a more pronounced perinuclear and nuclear localization pattern(Figure 3B).

(A)

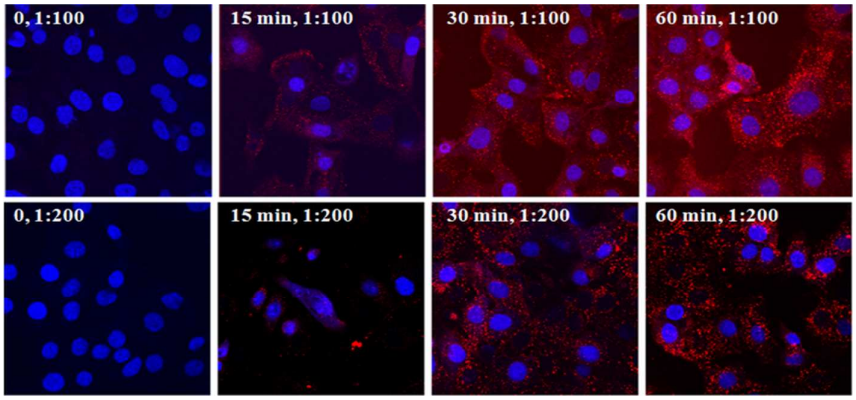

(B)

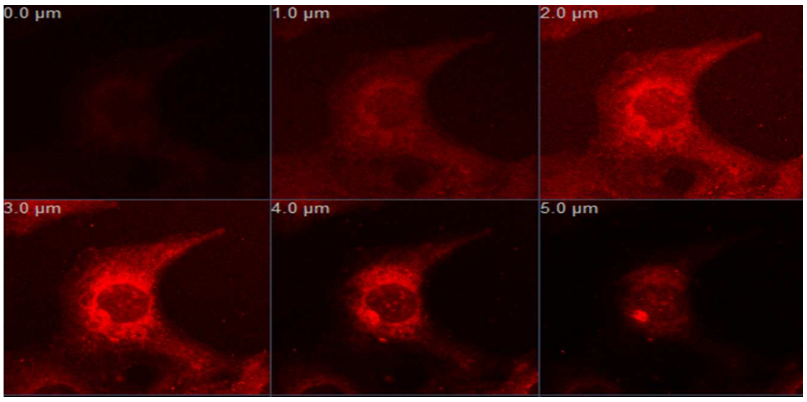

Figure 3. Intracellular uptake of NPs visualized by CLSM. (A) Intracellular uptake of PE Lissamine Rhodamine B-loaded NPs (red) by SKOV-3 cells was evaluated following 0-60min. incubation with two formulation dilutions 1:100 and 1:200, nuclei were stained with DAPI (blue). (B) Z-stack confocal

imaging of SKOV-3 cells incubated with PE Lissamine Rhodamine B-loaded NPs (red) for 6h (dilution 1:100).

2.5. In vivo evaluation of 1 and 2 for the treatment of solid tumors

For *in vivo* evaluation of **1**, **2** and OXA, the mice were divided into three treatment groups including: solution of **1** in polyoxyl-35 castor oil /ethanol diluted by 10 in water for injection, free OXA and control (polyoxyl-35 castor oil /ethanol diluted by 10 in water for injection), and **2**. In fact, when diluted in 90% water for injection, solution of **1** in polyoxyl-35 castor oil / ethanol produces micelles of approximately 13 nm diameter, indicating that the administered solution could behave like a transparent tiny suspension of micelle-type nanocarrier, with potential accumulation ability at RES organs and tumor tissue (Figure S2). A pharmacological evaluation was performed to verify the therapeutic superiority of **1** and **2** compared to OXA using a CCCD camera to detect the luminescence emitted from the tumor following luciferin i.p. administration. The tumor bioluminescence evaluation (at longitudinal view) of the tumor within the same groups of animals exhibit both sensitive and quantitative measurement of tumor response *in vivo*.

Metastatic ovarian tumors were induced by luciferase transfected SKOV3-luc-D3 cells injected into the peritoneal cavity of SCID-bg mice. Tumor development and progression was validated by bioluminescent imaging. Tumor signals from the images were quantified using LivingImage software version 4.3.1, and luminescence group averages were plotted over time. Thirty days following cells' injection, treatments were injected into the tail vein once a week over four weeks. It can be clearly seen from Figure 4A and D, that **1** and **2** were significantly most efficient in ovarian tumor growth inhibition in comparison to OXA and the control. Although the tumor was not completely eradicated, **1** and **2** reached the tumor more efficiently than the OXA, and

the subsequent therapeutic effect was significantly greater. Ventral images of a representative mouse from each group taken on weeks 4, 7, 9 and 10 following tumor inoculation are presented in Figure 4D. Importantly, no signs of systemic toxicities [weight loss (Figure 4B), weakness, pain or discomfort] and no local reactions at the injection site were observed following **1** and **2** administrations.

We were interested in evaluating the effect of larger tolerated doses of **1** than with OXA based on molar calculations. The molar equivalence dose of OXA (5mg/kg) for **1,** is 9mg/kg while the dose injected was 15mg/kg. However, the results of a small pilot study where 15mg/kg of **1** was compared to 9mg/kg equivalent to the dose injected of OXA of 5mg/kg, showed no significant difference in tumor growth inhibition and therefore it was decided to proceed with only 9mg/kg of **1** either in free solution or in NPs for the other cancer models.

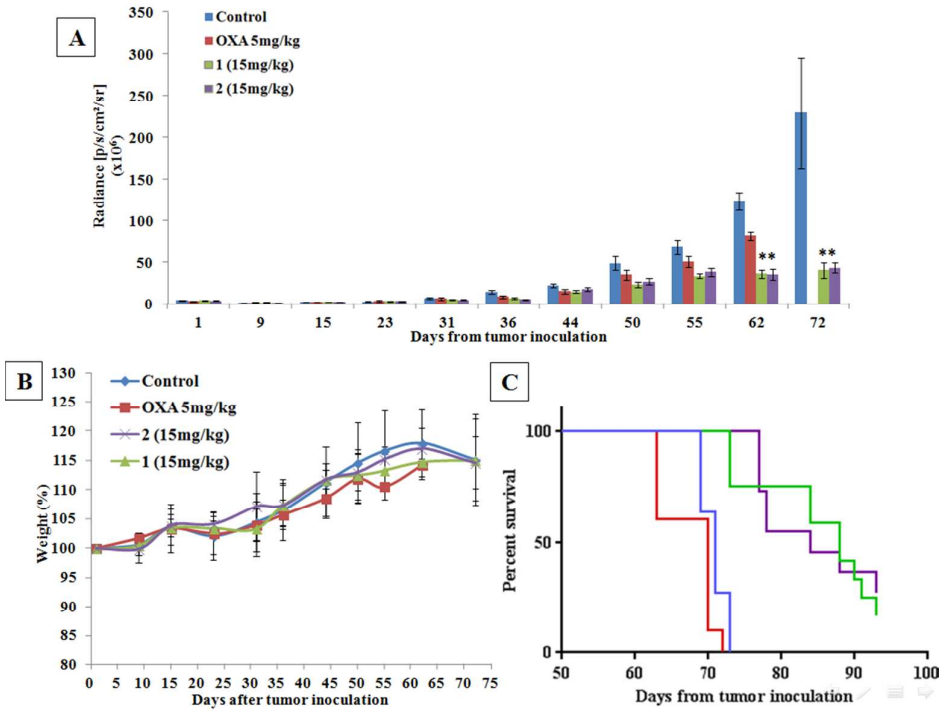

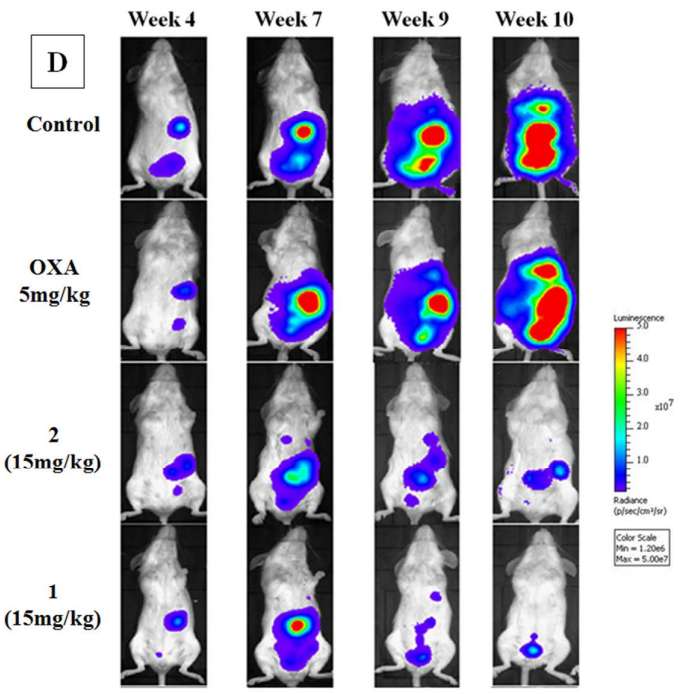

Figure 4. Efficacy study. (A) Longitudinal detection and quantification of SKOV3-luc-D3 ovarian tumor growth in live mice by the bioluminescent luciferase imaging assay using a CCCD camera. Tumor size is designated by the total luminescence intensity of the dorsal and ventral images, expressed in radiance units (photons/s/cm^2/sr). Arrows indicate the treatment schedules on the 30th, 37th, 45th and 52nd day. Results are presented as mean ± SE. Statistical analysis revealed that the observed differences at days 62 and 72 were significant ($p<0.01$, one-way ANOVA). Post hoc analysis showed that there are significant differences between the control group and **1** and **2** treatment groups [$p<0.01$, Dunnett test (2-sided)]. (B) Body weight follow-up beginning from tumor inoculation (day 0) through the study period. Changes were recorded as a percentage of the initial body weight observed on the day of tumor cells injection (100% at day 0). Results are presented as mean ± SD. (C) Kaplan-Meier survival curve from day of tumor cells injection until death. Death was recorded once animals fulfilled predetermined euthanasia criteria. **** $p < 0.0001$. The study was terminated on the 93rd day. (D) Representative ventral images of mice taken on weeks 4, 7, 9 and 10 following tumor inoculation are given.

Animals treated with **1** and **2** exhibited the longest survival rate compared to OXA and control groups (Figure 4C). On the 73rd day, 100% of mice in the **2** group were still alive, whereas all mice in the control and OXA groups had died and 75% survival proportions were recorded for the **1** group. The mean survival time in the **1** and **2** groups, as analyzed by the Kaplan–Meier statistics, was 88 and 84 days, respectively, whereas for OXA and the control the mean survivals were 70 and 71 days, respectively. Survival differences were statistically significant.

We next monitored the effect of **1**, **2** and OXA on tumor growth over time in a mouse xenograft model of colon cancer by noninvasive *in vivo* luminescence imaging. Mice were subcutaneously injected with HCT 116-luc2 cells, which stably expressed firefly luciferase, and treatment was administered once every fourth day by i.v. injection (tail) as described previously. There was an increase in tumor growth in the groups of the control and OXA. However, in the groups of **1** and **2** in an equivalent concentration to OXA, tumor growth was significantly impaired with a decrease in tumor volume as compared to the control (Figure 5A). In contrast to the other animal studies, the animals in the treated groups initially lost weight but recovered and even increased in weight with time (Figure 5B).

Animals treated with **2** exhibited the longest survival rate compared to other treatment groups (Figure 5C). On the 63rd day, 50% of mice in the **2** treatment group were still alive, whereas all mice in the **1**, control and OXA groups had died. The mean survival time in the **2** treatment group, as analyzed by the Kaplan–Meier statistics, was 69 days, whereas for **1**, OXA and control the mean survivals were 55, 55, and 47 days, respectively. Survival differences were statistically significant, even when **2** treated mice were only compared to **1** treated mice, reinforcing the added value provided by the nano-delivery system (Figure 5C).

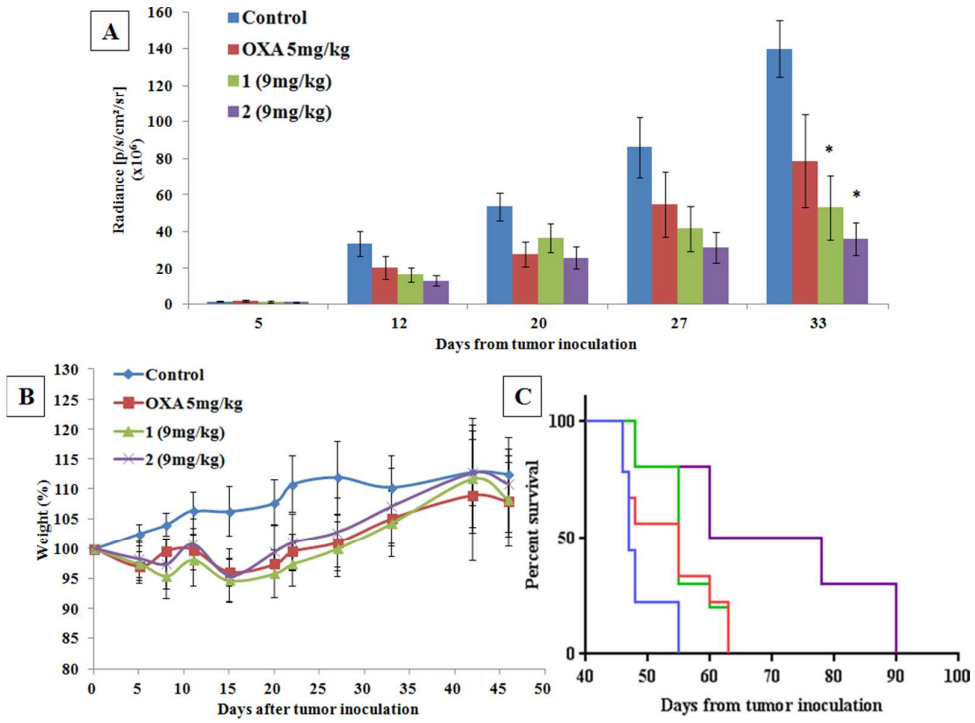

Figure 5. Efficacy study. (A) Longitudinal detection and quantification of HCT 116-luc2 colon tumor growth in live mice by the bioluminescent luciferase imaging assay using a CCCD camera. Tumor size is designated by the luminescence intensity of the dorsal images, expressed in radiance units (photons/s/cm^2/sr). Results are presented as mean ± SE. Statistical analysis revealed that the observed differences in radiance values on the 33rd day were significant ($p<0.01$, one-way ANOVA). Post hoc analysis showed significant differences between **1**, **2** and control on the 33rd day [$p<0.01$, Dunnett test (2-sided)], whereas there was no significant difference between OXA and control. (B) Body weight follow-up beginning from tumor inoculation (day 0) through the study period. Changes were recorded as a percentage of the initial body weight observed on the day of tumor cells injection (100% at day 0). Results are presented as mean ± SD. (C) Kaplan-Meier survival curve from tumor cells injection day until death. Death was recorded once animals fulfilled predetermined euthanasia criteria. **** $p < 0.0001$.

3. DISCUSSION

Pt-based complexes are widely used in the treatment of various solid tumors, although exhibiting serious side-effects. Furthermore, it is well known from the literature that the therapeutic outcome of Pt-based chemotherapy can be impaired by acquired

resistance which is one of the major limitations of Pt anticancer chemotherapy. The present study aimed to develop and characterize a drug delivery system loaded with a novel potent Pt(IV) prodrug of OXA for improved treatment of solid tumors.

Because of the drawbacks of Pt(II) drugs, there is an incentive to synthesize lipophilic Pt(IV) complexes in an attempt to improve efficacy and overcome resistance as already reported by other authors, while trying to enhance the lipophilicity of cisplatin [25-28] and OXA [29-31]. Due to their octahedral coordination geometry, platinum(IV) complexes are preferred over their platinum(II) counterparts. The presence of two additional ligands facilitates their ability to detect and attach to specified targets. In contrast to previous approaches, in which symmetric Pt(IV) compounds were designed with the aim of tuning lipophilicity [32-34], in the present study efforts concentrated on enhancing the lipophilicity of OXA using a different approach based on combining adversative ligands, by means of aqueous solubility and lipophilicity on the same Pt(IV) scaffold resulting in an asymmetric compound, namely **1**.

The antiproliferative activities of the OXA and **1** were assessed in several cancer cell lines, as depicted in Table 1. The cytotoxicity of **1** was substantially greater (more than two orders of magnitude) than that of OXA in both Pt sensitive and resistant cell lines, perhaps as a result of its enhanced accumulation because of its lipophilic character, as shown previously with other Pt compounds [29, 35-37].

Formulation **2** formed using the interfacial deposition method in the presence of lipoid E80 and OCA. PLGA was selected for this study because of its biocompatibility, biodegradability and FDA approval for biomedical applications [38]. The formed particles typically displayed a remarkable loading rate in contrast to other nanoparticulate formulations where low loading rates (less than 6%w/w) of the active

ingredients were obtained, confirming the adequate optimization of the actual formulation. Fatemeh *et al.* reported preparation of cisplatin and carboplatin-loaded polybutylcyanoacrylate NPs with loading percentages of 4 and 6 %, respectively [39]. Indeed, the low drug loading is common for Pt NPs, and can be attributed to their physico-chemical characteristics [40, 41].

It should be emphasized that in contrast to other studies [2, 42, 43] where the incorporation of Pt-based agents within NPs enhanced their cytotoxic activity owing to improved internalization, in the present case **1** displayed similar activity to **2**. This is apparently due to its lipophilic character and intrinsic properties of the free active molecule allowing for significant penetration within the cytosol as shown in Figure 2 where the amounts of **1** in the various cellular fractions were much higher than the amount of **2**, with the exception of the cytoskeletal fraction where the amount was not significantly different. A plausible explanation for why these differences in concentrations in the various cellular fractions are not reflected in the cytotoxic activity should be attributed to the gradual release of **1** from NPs over a prolonged period of time into the target nucleus and cytoskeletal fraction compensating for the smaller concentration which remains active. Moreover, an alternative explanation cannot be excluded, i.e. the formation of free **1** molecules assembling into large micelles following the preparation of **1** solution and dilution by cell culture media. Nevertheless, it is still worth continuing the development of **2** because the presence of two additional ligands in **1** modified the chemical properties compared with the parent drug (OXA), making it more lipophilic and difficult to formulate in an aqueous solution.

Delivery of a lipophilic drug to its target has always been a challenge and a subject of active research. The reduced solubility of drug molecules may hinder their ability to

cross the physiological aqueous environments encompassing a cell and to penetrate the cell membrane. Furthermore, complications such as embolisms and local toxicity are likely to occur if the lipophilic or hydrophobic molecules tend to precipitate once i.v. injected at the site of administration[44]. Thus, such compounds need to be formulated in surfactant solutions to enhance the solubility and prevent potential precipitation. However, it is known from literature that surfactant agents such as polyoxyl-35 castor oil and polysorbate 80, widely used in the marketed cytotoxic products, can cause many adverse effects including pain, inflammation, neutropenia, hypersensitivity and even anaphylactic shock [12, 15, 17]. Therefore, in the present case and in order to avoid the adverse effects normally elicited by these excipients as well as future complications, it was decided to formulate the novel compound in PLGA NPs. This is a promising approach to overcome the poor water solubility of a lipophilic drug, by encapsulation in a NP-based carrier. Additionally, in the present study it was anticipated that the incorporation of **1** in NPs would not enhance the cytotoxic activity by accumulation of drug-loaded NPs in the cancer cells via endocytosis, as already reported in other studies [45-47], because it was assumed that like other lipophilic prodrugs under dilution of the parent drug, it would form micellar nanocarriers per se [48]. Nevertheless, cellular internalization of NPs into cancer cells was observed within minutes and gradually increased (Figure 3).

Pt(II) complexes are kinetically labile, and one advantage of Pt(IV) prodrugs is their relatively greater kinetic inertness [4]. This reduced reactivity is expected to translate into prolonged circulation time *in vivo*, because of the protection of Pt(II) pharmacophore from deactivation by biological nucleophiles. Once the complex enters the reducing environment of the cancer cell, it should reduce, forming the active Pt(II) agent [49]. We propose that incorporation of **1** into NPs further protects it

from reduction by physically preventing interaction between reducing agents and the encapsulated **1**. It was recently reported that encapsulation of the Pt(IV) anticancer compound, mitaplatin, prolonged retention of Pt in the bloodstream more than unencapsulated mitaplatin. Moreover, while both mitaplatin alone and mitaplatin-loaded NPs displayed the same long-term tumor growth inhibition in mice carrying MDA-MB-468 triple-negative breast cancer xenografts, the nanodelivery of the Pt agent significantly shifted the biodistribution of Pt in treated animals away from accumulation in the kidneys, a traditional site of Pt-induced toxicity [50].

In the present study, an *in vivo* experiment was conducted, in which SKOV-3-luc cells were inoculated in SCID-bg mice. Due to the lack of an anatomical barrier between the ovaries and the peritoneal cavity, metastatic resistance of patients with ovarian cancer is severely reduced, and cancer cells are able to escape from the ovaries and form tumor nodules on the peritoneal surface[51]. To closely mimic the disease, we established an i.p. disease model by injecting SKOV-3 cells intraperitoneally and evaluating the efficacy of **1**, **2** and OXA accordingly. The antitumor activity of **1** and **2** indicated significantly decreased tumor growth compared to the control and OXA treatment groups (Figure 4).

The similar antitumor activity exhibited by **1** and **2** irrespective of the animal cancer model might be due to micelles formation resulting from dilution of **1** in polyoxyl-35 castor oil / ethanol solution in 90% water for injection, suggesting that the administered solution is in fact a micellar solution displaying an EPR effect (Figure S2). Additionally, *in vivo* findings reinforce *in vitro* results obtained for the tested cell lines (Table 1 and Figure 2), in which IC_{50} values of **1** and **2** were lower than those of OXA, and respective Pt accumulation values were significantly greater than OXA elicited values.

Moreover, animals treated with **1** and **2** exhibited the longest survival rate compared to OXA and control groups in animal models. In ovarian cancer model, on the 73rd day, 100% of mice in **2** treatment group were still alive, whereas all mice in the control and OXA groups had died and 75% survival proportions were recorded for **1** treatment group (Figure 4C). Moreover, on the 63rd day, 50% of mice in the **2** treatment group were still alive, whereas all mice in the **1**, control and OXA groups had died in the subcutaneous model of colon cancer (HCT-116) in SCID-bg mice (Figure 5C). These findings reinforce the advantage of **1** molecule per se and **2** over OXA in the treatment of ovarian and colon cancer. Tumor development and progression were also validated by bioluminescent imaging. The results revealed that **1** and **2** were equally and significantly more efficient in tumor growth inhibition compared to OXA and the control (Figure 5). It should be emphasized that **2** exhibited a remarkable survival advantage over other groups in the colon cancer animal model since the final surviving mouse lived for 90 days, whereas all the mice in the other groups survived up to 63 days, indicating the added value of **2** (Figure 5C). The findings of this study support the improved treatment hypothesis and substantially enhance tumor growth inhibition elicited by **1** and **2** over OXA, although no complete tumor eradication was achieved. This could be attributed to several factors, one being that the cancer cells applied in the *in vivo* experiments are of human origin, yielding very aggressive tumor models with a rapid growth rate, which is unlikely to be seen in the clinics. Indeed, while the efficacy of the novel complex as a single-agent therapy was demonstrated, combination therapy is the mainstay treatment of cancer in clinical practice, particularly for advanced stages of the disease. Moreover, the results of this study are encouraging and reveal considerable potential for further development of this formulation.

So far, only a few reports of nano delivery systems of OXA have been reported [52-55]. Among them, to the best of our knowledge, there are no reports describing the asymmetric Pt(IV) prodrug of OXA incorporated into PLGA nanospheres.

4. CONCLUSIONS

Pt drugs are still among the most essential drugs in chemotherapy, but their lack of cancer-cell selectivity leads to toxicity issues. Here we report a novel Pt(IV) prodrug of OXA, namely **1**, containing both lipophilic and hydrophilic axial ligands, with increased efficiency in killing cancer cells. The overall results indicate that **1** and **2** lead to significant tumor growth inhibition in comparison to OXA, and were effective in both orthotopic and xenograft tumor models. Moreover, complex **1** was incorporated in PLGA NPs delivery vehicles with the aim of mitigating the high systematic toxicity and severe side effects associated with Pt drugs. Such a NP treatment could become an attractive candidate for further investigation as a chemotherapeutic treatment for solid tumors.

5. EXPERIMENTAL SECTION

5.1. Materials

Oxaliplatin was acquired from AK Scientific, Inc. (Union City, CA, US); Cisplatin, Palmitic acid, polyoxyl-35 castor oil (Cremophor®EL) and Thiazolyl Blue Tetrazolium Bromide were purchased from Sigma-Aldrich (Jerusalem, Israel). Lipoid E80 was acquired from Lipoid GmbH (Ludwigshafen, Germany). PLGA (MW 50 kD, Resomer RG 504 H) was purchased from Boehringer Ingelheim GmbH (Ingelheim, Germany). Oleyl cysteineamide (OCA) was synthesized as published previously [48]**.** Solutol® HS 15 was donated by BASF (Ludwigshafen, Germany). Firefly D-luciferin, potassium salt was obtained from Regis Technologies, Morton Grove, IL, USA. All

organic solvents were HPLC grade and purchased from J.T Baker (Deventer, Holland). The PC-3, BxPC-3, OVCAR-8 and SKOV-3 cell lines were purchased from American Type Culture Collection (ATCC), Rockville, MD, USA. PC-3-luc, SKOV3-luc-D3, and HCT 116-luc2 were purchased from Caliper Life Sciences (Hopkinton, MA, USA). CT-26-luc cell line was kindly supplied by Dr. Gilad Bachrach from Hebrew University. A2780 and A2780-cisR cells line were kindly supplied by Prof. B. Keppler from University of Vienna. Most of the cells were purchased during the last three years and normally when received, they were de-freezed, subcultured according to the manufacturer protocol to the appropriate passage and stored as aliquots in liquid nitrogen. Every two months, the cells were tested for mycoplasma contamination according to the manufacturer protocol. All tissue culture products were from Biological Industries Ltd (Beit Ha Emek, Israel). Luciferase transfected cell lines were obtained from Caliper Life Sciences (Hopkinton, MA). Pt concentrations were determined by an Agilent 7500ce inductively coupled plasma mass spectroscopy (ICP-MS). Tumor signals from the images of *in vivo* studies were quantified using LivingImage software version 4.3.1.

5.2. Instrumentation

All NMR data were collected on a Bruker AVANCE IIITM HD 500 MHz spectrometer using a 500 Mhz SmartProbe. ^{195}Pt NMR data were collected at 107.47 MHz using sw= 217391.3 Hz aq=0.002sec and rd=0.001sec. The data were processed using MestreNova with a 300 Hz line broadening and backward linear prediction. ^{1}H spectra were recorded with standard parameters. Analytical HPLC analysis was performed on a standard Dionex UPLC system equipped with a Kinetex 5µ XB-C18 100A New Column 250x4.6mm with detection at 220nm. Preparative purification was carried out on a Dionex semi- preparative HPLC using Phenomenex Luna 10µ

C18 100A 250x21.20mm column at 220nm. Platinum concentrations were determined by an Agilent 7500ce inductively coupled plasma mass spectroscopy (ICP-MS). The mean diameter and the zeta potential of the NPs were characterized using Malvern's Zetasizer (Nano series, Nanos-ZS, UK) at 25°C and using water as diluent. Morphological evaluation was performed on carbon-coated Cu grids (300-mesh), using an electron microscope (CM12 TEM, Philips) at 100 kV, after negative staining using 2% uranyl acetate. Cellular uptake evaluation of NPs was done by Zeiss LSM 710 Spectral Confocal Laser Scanning Microscope (CLSM). MS analysis was performed with a TSQ Quantum Access Max mass spectrometer with a heated electrospray ionization (H-ESI) interface (Thermo Scientific, San Jose, CA, USA).

5.3. Synthesis and characterization of 1

5.3.1. Synthesis of [Pt(DACH)(OAc)(OH)(ox)]: OXA (1.5g, 3.8mmol) was taken in 100mL acetic acid and 50µL of 30% H_2O_2 was added. The reaction mixture was stirred at room temperature for 4-5h and the reaction was monitored by ^{195}Pt NMR. Excess acetic acid was removed by vacuum evaporation and the resulting white solid was washed with diethyl ether and acetone and dried under vacuum. The product was further purified by preparative HPLC (5%ACN:95% H_2O as mobile phase), RT= 7.6min. Yield: 1.456g, 80.94%. ^{195}Pt nmr (in acetic acid), δ (ppm)= +1389. ^{1}H NMR (D_2O) δ = 1.02-1.17(b,2H), 1.32-1.54(b,4H), 1.89(s,3H), 2.06-2.18 (B,2H), 2.66-2.75(b, 2H)

5.3.2. Synthesis of Palmitic anhydride: Palmitic acid (500mg, 1.95mmol) was dissolved in 20mL dichloromethane and N,N'-Dicyclohexylcarbodiimide (0.5eq., 201.2mg, 0.975mmol) was added. The reaction mixture was stirred at room temperature for 12h. Progress of the reaction was monitored by TLC with ethyl acetate as the mobile phase. N,N'-Dicyclohexylurea that formed was filtered off from

the reaction mixture and excess dichloromethane was removed by evaporation. The white solid obtained after the removal of dichloromethane was re-dissolved in a small amount of dichloromethane and the N,N'-Dicyclohexylurea that precipitated was filtered off again. This step was repeated four times to remove N,N'-Dicyclohexylurea completely. Palmitic anhydride was characterized by ^{1}H NMR. Yield: 858 mg 89%. ^{1}H NMR ($CDCl_3$): δ= 0.8-0.9(t,6H), 1.16-1.36(m,48H), 1.56-1.69(q,4H), 2.30-2.46(t, 4H).

*5.3.3. Synthesis of **1**:* [Pt(DACH)(OAc)(OH)(ox)] **(**1g, 2.1mmol) was dissolved in 5mL DMF and palmitic anhydride (1.57g. 3.17mmol) was added. The reaction mixture was stirred at 40°C overnight and monitored by ^{195}Pt NMR. Unreacted anhydride (precipitated upon cooling) was filtered off from the reaction mixture and DMF was removed by vacuum evaporation yielding a light-yellow solid. In order to purify the compound, 1mL methanol was added to the solid obtained after the evaporation of DMF and the mixture was shaken well. The insoluble white precipitate was collected by centrifugation and washed twice with small portions of methanol and dried in vacuum. The compound obtained was characterized by ^{195}Pt NMR and ^{1}H NMR**.** Yield**:** 1.156g, 76.97%, ^{195}Pt NMR (DMF) **δ=** 1589. ^{1}H NMR (DMSO-D6) δ =: 0.79-0.87(t,3H), 1.13-1.27(b,24H), 1.30-1.54(b,5H), 1.93(S,3H), 2.02-2.15(m,2H), 2.17 -2.28(m,2H), 2.76-2.94(b,2H), 8.20-8.6(b,4H). m/z (calculated) = 711.75, m/z (found)=712.19. The calculated elemental analysis for **1** is C, 43.87; H, 6.80; N, 3.94. The actual analysis of the prepared material was C, 43.69; H, 6.61; N, 3.89. HPLC chromatogram of **1** (100%Acetonitrile), RT= 3.6 min. According to these findings, the purity of **1** is higher than 98%. The purity of **1** was further confirmed by the HPLC method previously described in the instrumentation section following injection

of high concentrations (200 μg/ml). The purity was higher than 95% based on the various peaks areas detected in the chromatogram.

5.4. Cell lines and cell incubation conditions

All cell culture mediums and all the cell lines were tested and authenticated from any mycoplasma contamination. A Mycoplasma contamination test was done prior to the use of cells by a polymerase chain reaction (PCR) method (EZ-PCR Mycoplasma kit, Biological Industries, Israel). The *in vitro* experiments were performed in human cell lines of prostate cancer (PC-3 and PC-3-luc), pancreatic cancer (BxPC-3), ovarian cancer (SKOV-3, A2780, A2780-cisR and OVCAR-8), and murine colorectal cancer CT-26-luc cells. BxPC-3 and OVCAR-8 cells were grown in RPMI medium supplemented with 10% fetal bovine serum (Gibco), 1% L-glutamine, 100U/mL penicillin, 100ug/mL streptomycin and 0.13% w/w gentamycin. PC-3 and PC-3-luc cells were cultured in DMEM plus 10% fetal bovine serum, 1% L-glutamine, 100U/mL penicillin, 100μg/mL streptomycin and 1% pyrovate. SKOV-3 cells were cultured in McCoy's 5A medium supplemented with 10% fetal bovine serum, 100U/mL penicillin, and 100ug/mL streptomycin. A2780 and A2780-cisR cells were grown in RPMI medium supplemented with 10% fetal bovine serum, 1% L-glutamine and 0.1% w/w gentamycin, and the acquired resistance in A2780-cisR cell line was maintained by supplementing the medium with 1uM of cisplatin every second passage. CT-26-luc cells were grown in RPMI supplemented with 10% fetal bovine serum, 1% L-glutamine, 100U/mL penicillin, 100ug/mL streptomycin, and 100ug/mL neomycin. SKOV3-luc-D3 and HCT 116-luc2 cells were cultured in McCoy's 5A medium supplemented with 10% heat inactivated fetal bovine serum, 100U/mL penicillin, and 100ug/mL streptomycin.

The cell lines were maintained at 37°C under a moist atmosphere containing 5% CO_2 and 95% air. All cell culture products were obtained from Biological Industries (Beit Ha Emek, Israel).

5.5. Preparation and characterization of 2

*5.5.1. Preparation of **2***

Formulation **2** was prepared using the solvent deposition method [22]. Briefly, 7mg of **1**, 14mg PLGA 50kDa, 7mg lipoid E80 and 1.5mg Oleyl cysteineamide (OCA) were dissolved in 4mL (1:20) ethanol/acetone mixture. The organic phase was added to 2.5mL aqueous solution containing 0.1% w/v Solutol® HS 15. The suspension was stirred at 900rpm over 15min, and then concentrated by solvents' evaporation to a final volume of 2.5mL, followed by centrifugation for 10min at 4400rpm.

The resulting drug-loaded NPs consisted of spherical nanomatrices of PLGA, lipoid E-80 and OCA embedding **1**, and dispersed in 0.1% of Solutol HS15, solution were entitled **2**.

*5.5.2. Content determination of **1** in NPs*

To determine the amount of drug loaded in the NPs, formulation **2** was dissolved in acetonitrile and the drug concentration was determined using analytical Dionex HPLC system equipped with a Kinetex 5u XB-C18 100A Column 250x4.6mm. **1** was detected at a wavelength of 220nm. Acetonitrile 100% was used as a mobile phase and the flow rate was 1mL/min.

5.5.3. Physicochemical and morphological characterization

The particle size distribution and zeta potential of **2** were characterized by dynamic light scattering (DLS, Malvern Zetasizer Nano ZS, UK). Morphological and size evaluation of **2** was carried out using XHR SEM (model: Magellan 400L, FEI, Germany). The samples were fixed on a SEM-stub using double-sided adhesive tape and then made electrically conductive following standard coating by gold sputtering (Pilaron E5100) under vacuum. Morphological evaluation of the NPs was performed on carbon-coated Cu grids (300-mesh), using an electron microscope (CM12 TEM, Philips) at 100kV, after negative staining using 2% uranyl acetate. A diluted suspension of **2** ($1{:}1x10^6$) in water (HPLC grade, Baker) was placed onto the surface of cover glass (Marienfeld cover glass, 100, 22 x 22 mm). Samples were left to dry. The morphology and surface states were investigated using Scanning Probe Microscope Dimension 3100, Nanoscope V (Veeco, CA, USA).

*5.5.4. Lyophilization of **2***

Finally, to ensure the prolonged physical stability of the NPs, five types of sugars were evaluated as cryo- and lyoprotectants for the freeze-drying process of **2**: sucrose, (+) trehalose, D (-) mannitol, xylitol, and hydroxypropyl-β-cyclodextrin (HPβCD). The NP suspension was freeze-dried using an Epsilon 2-6d Martin Christ lyophilizer (Gef., Germany) to obtain a dry powder.

5.6. In vitro cytotoxicity assay

Cytotoxicity was determined by the colorimetric MTT (3-(4,5-dimethylthiazol-2-yl)-2,5 diphenyltetrazolium bromide) assay as described previously[48]. In brief, cells were seeded in a sterile, 24-well plate and incubated in the presence of the drug for 120h at 37°C, 5% CO_2. In the first 24h the cells were allowed to settle and resume exponential growth. Then, cells were incubated for 120h with treatments dispersed in full growth

medium at different drug concentrations (0-50μg/mL). Cells were extensively washed with HBSS and incubated with MTT solution (0.5mg/ml) in HBSS, 2, 37°C). Following another washing step, the dye was solubilized with DMSO and the absorbance was determined at 540nm.

5.7. Determination of platinum accumulation in whole cell

SKOV-3 cells were seeded in triplicate 24-well plates ($50x10^3$ cell/well), allowed to reach 80–90% confluence, and treated with OXA, **1** and **2** at concentrations of 35μM for 24h at 37°C. Following incubation, the drug-containing medium was removed, and cells were rinsed twice with cold PBS. The cells were harvested and centrifuged into a pellet. 1mL of concentrated nitric acid was added to cell pellets, and incubated at 70°C on a hot plate until the samples dried. The samples were dissolved in 0.1% SDS and 1% nitric acid, and analyzed for Pt content by ICP-MS. Protein concentration analysis was conducted by BCA assay. Briefly, the cells were incubated in the same mentioned conditions and concentrations. Following incubation, the drug-containing medium was removed, and each well was rinsed twice with cold PBS, trypsinized, and the cells were centrifuged into a pellet (4400rpm, 5min). The pellet was rinsed one more time with PBS and NaOH (0.1N) was added. After diluting the samples using water, they were incubated at 70ºC for 1h and the absorbance was measured at 562nm. The protein concentration of the sample was calculated according to the BSA standard curve.

5.8. Determination of platinum content binding to DNA (DNA platination)

SKOV-3 cells were seeded in triplicate 24-well plates ($50x10^3$ cell/well), allowed to reach 80–90% confluence, and treated with OXA, **1** and **2** at concentrations of

25μg/mL for 24h at 37°C. Following incubation, the drug-containing medium was removed, and cells were rinsed twice with cold PBS. The cells were harvested and centrifuged into a pellet (4400rpm, 5min). Genomic DNA was isolated using Qiagen DNeasy® Blood & Tissue Kit (Qiagen, Valencia, CA, USA) as per the manufacturer's instructions. The quantity of DNA was determined by Uvikon XS spectrophotometer (Secomam, France) from the absorption at 260nm. Triplicate runs were performed to determine the content of Pt in DNA.

Upon determination of the DNA concentration, the remaining solution was overnight wet ashed in 1% nitric acid at 70°C and analyzed for Pt content by ICP-MS. DNA platination was expressed as ng Pt/μg DNA.

5.9. Cellular distribution into different subcellular compartments

SKOV-3 cells were seeded in triplicate 24-well plates at a density of $50x10^3$ cell/well, and allowed to reach 80–90% confluence, then treated with the compounds (35μM) for 24h. Following incubation, the drug-containing medium was removed, and cells were rinsed twice with cold PBS. Cellular distribution into the different cell fractions (cytosol, nucleus, membrane/particulate, and cytoskeleton) was performed using a Fraction PREP cell fractionation kit from BioVision (Mountain View, CA), as per the manufacturer's instructions. Final Pt content was determined by inductively coupled plasma mass spectroscopy (ICP-MS).

5.10. Cellular Uptake Evaluation of NPs by Confocal Laser Scanning Microscopy (CLSM)

NPs were prepared as described earlier, with the addition of 200μg Egg Liss Rhod PE into the organic phase. SKOV-3 cells were seeded in full growth medium on μ-Slide 8 well (ibidi GmbH, Germany) (50,000 cells/0.2mL/well). Cells were grown for 24h

until sub-confluence and washed with PBS (37°C, 2 mM $MgCl_2$). Cells were incubated with the formulations at 37°C in serum-free medium over 0, 15, 30 and 60min, then washed extensively using PBS with $MgCl_2$ and fixated with 4% formaldehyde in PBS for 15min at room temperature (0.2mL/well). Cells were washed again, and nucleus stained using 4′,6-diamidino-2-phenylindole (DAPI) 10μg/mL in PBS for 5min (0.2mL/well), washed by PBS and then mounted with 20μl fresh DABCO solution in glycerol and visualized by CLSM.

5.11. In vivo evaluation of 1 and 2 for the treatment of solid tumors

Strict animal care procedures set forth by The Authority for Biological and Biomedical Models of the Hebrew University of Jerusalem based on guidelines from the NIH guide for the Care and Use of Laboratory Animals were followed (approval No. MD-13-13707-5).

5.11.1. Bioluminescent imaging and efficacy determination in an orthotopic intraperitoneal model of metastatic ovarian cancer in SCID-bg mice

Mice used were severe combined immunodeficiency female (SCID)-bg, 5-6 weeks old (Harlan, Jerusalem, Israel). Luciferase transfected SKOV3-luc-D3 cells (2×10^6 cells in 100 μL PBS) were injected directly into i.p. cavity of mice. For tumor validation and tumor growth follow up, bioluminescent imaging was performed every 7 days using a CCCD camera (IVIS, Caliper Life Sciences, Xenogen Corporation) as previously described[48]. Firefly D-luciferin was injected intraperitoneally and mice were anesthetized using 3% isoflurane. Animals were placed onto black paper in the IVIS imaging box and imaged dorsally and ventrally. Total luminescence (dorsal and ventral) was recorded in radiance units (photons/s/cm^2/sr). Thirty days following cells' injection and validation of tumor inoculation, mice were divided into four groups with

equal average radiance values (n = 10-12). The following 4 formulations were tested: Control (polyoxyl-35 castor oil /ethanol diluted by 10 in water for injection), free OXA at a dose of 5mg/kg, **1** in polyoxyl-35 castor oil /ethanol diluted by 10 in water for injection (15 mg/kg) and **2** (15 mg/kg). Treatments were injected into the tail vein once a week for four weeks.

5.11.2. Bioluminescent imaging and efficacy determination in a subcutaneous xenograft model of colon cancer in SCID-bg mice.

Mice used were severe combined immunodeficiency male (SCID)-bg, 5-6 weeks old (Harlan, Jerusalem, Israel). Luciferase transfected HCT 116-luc2 cells (1×10^6 cells in 100 μL PBS) were subcutaneously injected in the dorsal flank of mice. For tumor validation and tumor growth follow up, bioluminescent imaging was performed every 7 days using a CCCD camera (IVIS, Caliper Life Sciences, Xenogen Corporation). Firefly D-luciferin was injected intraperitoneally and mice were anesthetized by 3% isoflurane. Animals were placed onto black paper in the IVIS imaging box and imaged dorsally. Luminescence was recorded in radiance units (photons/s/cm^2/sr). One day following tumor inoculation, mice were randomly divided into the following treatment groups (n = 9-10). The same four formulations were tested: Control (polyoxyl-35 castor oil /ethanol diluted by 10 in water for injection), free OXA at a dose of 5mg/kg, **1** in polyoxyl-35 castor oil /ethanol diluted by 10 in water for injection (9 mg/kg) and **2** (9 mg/kg). Treatments were injected into the tail vein once every fourth day, four treatments in total.

In the two animal studies, mice were euthanized according to strict pre-determined criteria set by the Ethical Committee of the Animals' Authority.

5.12. Statistical analysis

Statistical analysis was performed with IBM SPSS Statistics Software version 22. One-way ANOVA was used to determine the difference between treatments, followed by the Tukey or Dunnett (2-sided) test. Statistical analysis of Kaplan–Meier statistics was performed using GraphPad Prism software version 6.07. Differences were considered significant if $p < 0.05$.

ASSOCIATED CONTENT

Supporting Data

IC_{50} (μM) and resistant factor values for OXA and **1** against A2780, A2780-cisR cell lines are presented, as well as IC_{50} values of OXA, **1**, and **2** in cancer cell lines used in the efficacy animal studies. Furthermore, DLS particle size distribution of **1** NPs spontaneously formed following dilution of **1** solution in DMSO by DDW at the same concentration as used for the cell culture experiments is shown. Moreover, the freeze drying parameters and characterization of lyophilized NPs after various time periods are also depicted. Finally, the ^{1}H and ^{195}Pt NMR spectra, HPLC chromatograms and ESI-MS spectra of complexes 1 used in this study are provided herein.

Corresponding authors

* S.B.: Tel. +97226758668, E-mail: simonb@ekmd.huji.ac.il,. T.N.: Tel. +97226757620, E-mail: tahern@ekmd.huji.ac.il.

† T.N and S.B. contributed equally.

Notes

The authors declare no competing financial interest.

Acknowledgements

The authors gratefully acknowledge Prof. Reuven Reich for providing excellent technical assistance in orthotopic intraperitoneal model of metastatic ovarian cancer, and Ofir Tirosh for long hours and hard work on the ICP-MS. DG thanks the Israel Science Foundation (grant 1611/14) for partial support.

Abbreviations

CLSM, Confocal Laser Scanning Microscopy; DDW, Double-distilled water; DLS, Dynamic Light Scattering; $IC_{50,}$ The 50% growth inhibitory concentration; ICP-MS; Inductively coupled plasma mass spectroscopy**;** OCA, Oleyl cysteineamide**;** OXA, Oxaliplatin; PDI, Polydispersity Index; SD, Standard Deviation; SE, Standard Error of the Mean; TEM, Transmission Electron Microscopy.

REFERENCES

1. Akbarzadeh, A.; Mikaeili, H.; Zarghami, N.; Mohammad, R.; Barkhordari, A.; Davaran, S. Preparation and in vitro evaluation of doxorubicin-loaded Fe(3)O(4) magnetic nanoparticles modified with biocompatible copolymers. *Int. J. Nanomedicine* **2012,** *7*, 511-526.

2. Oberoi, H. S.; Nukolova, N. V.; Kabanov, A. V.; Bronich, T. K. Nanocarriers for delivery of platinum anticancer drugs. *Adv. Drug Deliv. Rev.* **2013,** *65*, 1667-1685.

3. Kelland, L. The resurgence of platinum-based cancer chemotherapy. *Nat. Rev. Cancer* **2007,** *7,* 573-584.

4. Hall, M. D.; Mellor, H. R.; Callaghan, R.; Hambley, T. W. Basis for design and development of platinum(IV) anticancer complexes. *J. Med. Chem.* **2007,** *50*, 3403-3411.

5. Reithofer, M. R.; Bytzek, A. K.; Valiahdi, S. M.; Kowol, C. R.; Groessl, M.; Hartinger, C. G.; Jakupec, M. A.; Galanski, M.; Keppler, B. K. Tuning of lipophilicity and cytotoxic potency by structural variation of anticancer platinum(IV) complexes. *J. Inorg. Biochem.* **2011,** *105*, 46-51.

6. Giandomenico, C. M.; Abrams, M. J.; Murrer, B. A.; Vollano, J. F.; Rheinheimer, M. I.; Wyer, S. B.; Bossard, G. E.; Higgins, J. D. Carboxylation of kinetically inert platinum(IV) hydroxy complexes. An entr.acte.ee into orally active platinum(IV) antitumor agents. *Inorg. Chem.* **1995,** *34*, 1015-1021.

7. Galanski, M.; Keppler, B. K. Carboxylation of dihydroxoplatinum(IV) complexes via a new synthetic pathway. *Inorg. Chem.* **1996,** *35*, 1709-1711.

8. Gibson, D. The mechanism of action of platinum anticancer agents--what do we really know about it? *Dalton Trans.* **2009**, *48*, 10681-10689.

9. Loh, S. Y.; Mistry, P.; Kelland, L. R.; Abel, G.; Harrap, K. R. Reduced drug accumulation as a major mechanism of acquired resistance to cisplatin in a human ovarian carcinoma cell line: circumvention studies using novel platinum (II) and (IV) ammine/amine complexes. *Br. J. Cancer* **1992,** *66*, 1109-1115.

10. Moeller, N.; Kangarloo, B. S.; Puscasu, I.; Mock, C.; Krebs, B.; Wolff, J. E. Rational design of platinum chemotherapeutic drugs: hydrophobicity increases cytotoxicity. *Anticancer Res.* **2000,** *20*, 4435-4439.

11. Tallen, G.; Mock, C.; Gangopadhyay, S. B.; Kangarloo, B.; Krebs, B.; Wolff, J. E. Overcoming cisplatin resistance: design of novel hydrophobic platinum compounds. *Anticancer Res.* **2000,** *20*, 445-449.

12. Gelderblom, H.; Verweij, J.; Nooter, K.; Sparreboom, A. Cremophor EL: the drawbacks and advantages of vehicle selection for drug formulation. *Eur. J. Cancer* **2001,** *37,* 1590-1598.

13. Savjani, K. T.; Gajjar, A. K.; Savjani, J. K. Drug solubility: importance and enhancement techniques. *ISRN Pharm.* **2012,** 2012, 195727.

14. Shin, H. C.; Alani, A. W. G.; Rao, D. A.; Rockich, N. C.; Kwon, G. S. Multidrug loaded polymeric micelles for simultaneous delivery of poorly soluble anticancer drugs. *J. Control Release* **2009,** 140 (3) 294 -300.

15. Gradishar, W. J. Albumin-bound paclitaxel: a next-generation taxane. *Expert Opin. Pharmacother.* **2006,** *7*, 1041-1053.

16. Ma, Y.; Zheng, Y.; Zeng, X.; Jiang, L.; Chen, H.; Liu, R.; Huang, L.; Mei, L. Novel docetaxel-loaded nanoparticles based on PCL-Tween 80 copolymer for cancer treatment. *Int. J. Nanomedicine* **2011,** *6*, 2679-2688.

17. Ten Tije, A. J.; Verweij, J.; Loos, W. J.; Sparreboom, A. Pharmacological effects of formulation vehicles : implications for cancer chemotherapy. *Clin. Pharmacokinet.* **2003,** *42*, 665-685.

18. Gabano, E.; Ravera, M.; Osella, D. Pros and cons of bifunctional platinum(IV) antitumor prodrugs: two are (not always) better than one. *Dalton Trans.* **2014,** *43*, 9813-9820.

19. Xu, X.; Ho, W.; Zhang, X.; Bertrand, N.; Farokhzad, O. Cancer nanomedicine: from targeted delivery to combination therapy. *Trends Mol. Med.* **2015,** *21*, 223-232.

20. Rizzo, L. Y.; Theek, B.; Storm, G.; Kiessling, F.; Lammers, T. Recent progress in nanomedicine: therapeutic, diagnostic and theranostic applications. *Curr. Opin. Biotechnol.* **2013,** *24*, 1159-1166.

21. Mahapatro, A.; Singh, D. K. Biodegradable nanoparticles are excellent vehicle for site directed in-vivo delivery of drugs and vaccines. *J. Nanobiotechnology* **2011,** *9*, 55.

22. Fessi, H.; Puisieux, F.; Devissaguet, J. P.; Ammoury, N.; Benita, S. Nanocapsule formation by interfacial polymer deposition following solvent displacement. *Int. J. Pharm.* **1989,** *55*, R1-R4.

23. Byrne, J. D.; Betancourt, T.; Brannon-Peppas, L. Active targeting schemes for nanoparticle systems in cancer therapeutics. *Adv. Drug Deliv. Rev.* **2008,** *60*, 1615-1626.

24. Abdelwahed, W.; Degobert, G.; Stainmesse, S.; Fessi, H. Freeze-drying of nanoparticles: formulation, process and storage considerations. *Adv. Drug Deliv. Rev.* **2006,** *58*, 1688-1713.

25. Zheng, Y. R.; Suntharalingam, K.; Johnstone, T. C.; Yoo, H.; Lin, W.; Brooks, J. G.; Lippard, S. J. Pt(IV) prodrugs designed to bind non-covalently to human serum albumin for drug delivery. *J. Am. Chem. Soc.* **2014,** *136*, 8790-8798.

26. Graf, N.; Bielenberg, D. R.; Kolishetti, N.; Muus, C.; Banyard, J.; Farokhzad, O. C.; Lippard, S. J. alpha(V)beta(3) integrin-targeted PLGA-PEG nanoparticles for enhanced anti-tumor efficacy of a Pt(IV) prodrug. *ACS Nano* **2012,** *6*, 4530-4539.

27. Varbanov, H.; Valiahdi, S. M.; Legin, A. A.; Jakupec, M. A.; Roller, A.; Galanski, M.; Keppler, B. K. Synthesis and characterization of novel bis(carboxylato)dichloridobis(ethylamine)platinum(IV) complexes with higher cytotoxicity than cisplatin. *Eur. J. Med. Chem.* **2011,** *46*, 5456-5464.

28. Zak, F.; Turanek, J.; Kroutil, A.; Sova, P.; Mistr, A.; Poulova, A.; Mikolin, P.; Zak, Z.; Kasna, A.; Zaluska, D.; Neca, J.; Sindlerova, L.; Kozubik, A. Platinum(IV) complex

with adamantylamine as nonleaving amine group: synthesis, characterization, and in vitro antitumor activity against a panel of cisplatin-resistant cancer cell lines. .*J Med. Chem.* **2004,** *47*, 761-763.

29. Neumann, W.; Crews, B. C.; Sarosi, M. B.; Daniel, C. M.; Ghebreselasie, K.; Scholz, M. S.; Marnett, L. J.; Hey-Hawkins, E. Conjugation of cisplatin analogues and cyclooxygenase inhibitors to overcome cisplatin resistance. *Chem. Med. Chem.* **2015,** *10*, 183-192.

30. Novohradsky, V.; Zerzankova, L.; Stepankova, J.; Vrana, O.; Raveendran, R.; Gibson, D.; Kasparkova, J.; Brabec, V. Antitumor platinum(IV) derivatives of oxaliplatin with axial valproato ligands. *J. Inorg. Biochem.* **2014,** *140*, 72-79.

31. Zhang, J. Z.; Wexselblatt, E.; Hambley, T. W.; Gibson, D. Pt(IV) analogs of oxaliplatin that do not follow the expected correlation between electrochemical reduction potential and rate of reduction by ascorbate. *Chem. Commun. (Camb)* **2012,** *48*, 847-849.

32. Khokhar, A. R.; al-Baker, S.; Shamsuddin, S.; Siddik, Z. H. Chemical and biological studies on a series of novel (trans-(1R,2R)-, trans-(1S,2S)-, and cis-1,2-diaminocyclohexane)platinum(IV) carboxylate complexes. *J. Med. Chem.* **1997,** *40*, 112-116.

33. Kelland, L. R.; Murrer, B. A.; Abel, G.; Giandomenico, C. M.; Mistry, P.; Harrap, K. R. Ammine/amine platinum(IV) dicarboxylates: a novel class of platinum complex exhibiting selective cytotoxicity to intrinsically cisplatin-resistant human ovarian carcinoma cell lines. *Cancer Res.* **1992,** *52*, 822-828.

34. Ellis, L. T.; Er, H. M.; Hambley, T. W. The Influence of the axial ligands of a series of platinum(IV) anti-cancer complexes on their reduction to platinum(II) and reaction with DNA. *Aust. J. Chem.* **1995,** *48*, 793 - 806

35. Cui, H.; Goddard, R.; Porschke, K. R.; Hamacher, A.; Kassack, M. U. Bispidine analogues of cisplatin, carboplatin, and oxaliplatin. synthesis, structures, and cytotoxicity. *Inorg. Chem.* **2014,** *53*, 3371-3384.

36. Buss, I.; Kalayda, G. V.; Lindauer, A.; Reithofer, M. R.; Galanski, M.; Keppler, B. K.; Jaehde, U. Effect of reactivity on cellular accumulation and cytotoxicity of oxaliplatin analogues. *J. Biol. Inorg. Chem.* **2012,** *17*, 699-708.

37. Kozubik, A.; Vaculova, A.; Soucek, K.; Vondracek, J.; Turanek, J.; Hofmanova, J. Novel anticancer platinum(IV) complexes with adamantylamine: their efficiency and innovative chemotherapy strategies modifying lipid metabolism. *Met. Based Drugs* **2008,** 2008, 417897.

38. Karra, N.; Benita, S. The ligand nanoparticle conjugation approach for targeted cancer therapy. *Curr. Drug Metab.* **2012,** *13*, 22-41.

39. Fatemeh, D. R.; Ebrahimi Shahmabadi, H.; Abedi, A.; Alavi, S. E.; Movahedi, F.; Koohi Moftakhari Esfahani, M.; Zadeh Mehrizi, T.; Akbarzadeh, A. Polybutylcyanoacrylate nanoparticles and drugs of the platinum family: last status. *Indian J Clin. Biochem.* **2014,** *29*, 333-338.

40. Avgoustakis, K.; Beletsi, A.; Panagi, Z.; Klepetsanis, P.; Karydas, A. G.; Ithakissios, D. S. PLGA-mPEG nanoparticles of cisplatin: in vitro nanoparticle degradation, in vitro drug release and in vivo drug residence in blood properties. *J. Control Release* **2002,** *79*, 123-135.

41. Aryal, S.; Hu, C. M.; Zhang, L. Polymer--cisplatin conjugate nanoparticles for acid-responsive drug delivery. *ACS Nano* **2010,** *4*, 251-258.

42. Brown, S. D.; Nativo, P.; Smith, J. A.; Stirling, D.; Edwards, P. R.; Venugopal, B.; Flint, D. J.; Plumb, J. A.; Graham, D.; Wheate, N. J. Gold nanoparticles for the improved anticancer drug delivery of the active component of oxaliplatin. *J. Am. Chem. Soc.* **2010,** *132*, 4678-4684.

43. Paraskar, A.; Soni, S.; Roy, B.; Papa, A. L.; Sengupta, S. Rationally designed oxaliplatin-nanoparticle for enhanced antitumor efficacy. *Nanotechnology* **2012,** *23*, 075103.

44. Owen, S. C.; Doak, A. K.; Wassam, P.; Shoichet, M. S.; Shoichet, B. K. Colloidal aggregation affects the efficacy of anticancer drugs in cell culture. *ACS Chem. Biol.* **2012,** *7*, 1429-1435.

45. Oh, N.; Park, J. H. Endocytosis and exocytosis of nanoparticles in mammalian cells. *Int. J. Nanomedicine* **2014,** *9* Suppl 1, 51-63.

46. Sahay, G.; Alakhova, D. Y.; Kabanov, A. V. Endocytosis of nanomedicines. *J. Control Release* **2010,** *145*, 182-195.

47. Zhang, S.; Li, J.; Lykotrafitis, G.; Bao, G.; Suresh, S. Size-dependent endocytosis of nanoparticles. *Adv. Mater.* **2009,** *21*, 419-424.

48. Karra, N.; Nassar, T.; Ripin, A. N.; Schwob, O.; Borlak, J.; Benita, S. Antibody conjugated PLGA nanoparticles for targeted delivery of paclitaxel palmitate: efficacy and biofate in a lung cancer mouse model. *Small* **2013,** *9*, 4221-4236.

49. Hall, M. D.; Hambley, T. W. Platinum(IV) antitumour compounds: their bioinorganic chemistry. *Coord. Chem. Rev.* **2002**, *232* (1-2), 49-67.

50. Johnstone, T. C.; Kulak, N.; Pridgen, E. M.; Farokhzad, O. C.; Langer, R.; Lippard, S. J. Nanoparticle encapsulation of mitaplatin and the effect thereof on in vivo properties. *ACS Nano* **2013,** *7*, 5675-5683.

51. Bast, R. C., Jr.; Hennessy, B.; Mills, G. B. The biology of ovarian cancer: new opportunities for translation. *Nat. Rev. Cancer* **2009,** *9*, 415-428.

52. Sankhala KK, Mita AC, Adinin R, Wood L, Beeram M, Bullock S, Yamagata N, Matsuno K, Fujisawa T, Phan A. A phase I pharmacokinetic (PK) study of MBP-426, a novel liposome encapsulated oxaliplatin. *J. Clin. Oncol.* **2009**; *27*(15S): 2535.

53. Murakami, M.; Cabral, H.; Matsumoto, Y.; Wu, S.; Kano, M. R.; Yamori, T.; Nishiyama, N.; Kataoka, K. Improving drug potency and efficacy by nanocarrier-mediated subcellular targeting. *Sci. Transl. Med.* **2011,** *3*, 64ra2.

54. Campone, M.; Rademaker-Lakhai, J. M.; Bennouna, J.; Howell, S. B.; Nowotnik, D. P.; Beijnen, J. H.; Schellens, J. H. Phase I and pharmacokinetic trial of AP5346, a DACH-platinum-polymer conjugate, administered weekly for three out of every 4 weeks to advanced solid tumor patients. *Cancer Chemother. Pharmacol.* **2007,** *60*, 523-533.

55. Yang, C.; Liu, H. Z.; Lu, W. D.; Fu, Z. X. PEG-liposomal oxaliplatin potentialization of antitumor efficiency in a nude mouse tumor-xenograft model of colorectal carcinoma. *Oncol. Rep.* **2011,** *25*, 1621-168.

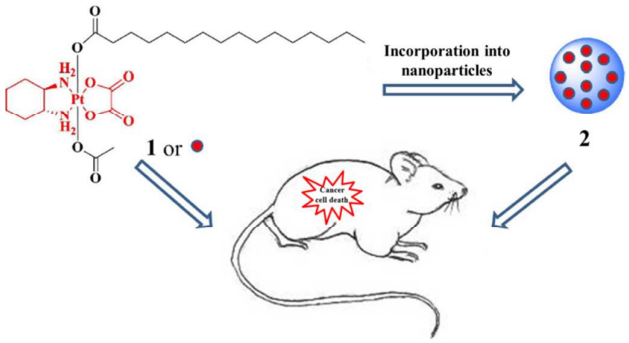

Table of Contents Graphic